LCLS-II Beam Dumps*

J. Welch, J. Blaha, P. Cutino, D. Hanquist, A. Ibrahimov, M. Kosovsky, Z. Li, M. Santana

October 18, 2017

Contents

List of Tables

*Work supported in part by the DOE Contract DE-AC02-76SF00515. This work was performed in support of the LCLS-II project at SLAC.

1 Introduction

We describe the complete beam dump systems for LCLS-II. Starting from requirements, we cover the design (including design of the cooling system, planned operation, and installation and removal), the calculated performance (including failure modes), and state the "rated" performance in terms of maximum beam power.

The starting point for the design is the overall performance required by LCLS-II and listed in Table 1 for two undulator dumps, DUMPS and DUMPH, and the BSY dump DUMPBSY [2, 3]. Various schemes were studied, including the use of the existing D10 dump/collimator for the DUMPBSY [4, 5], an aluminum sphere/water- style water dump for all dumps, and a dump with a solid aluminum core with edge cooling for the undulator dumps. The most critical design issues were to minimize the hazardous effects of radiation, both prompt and long term, and to obtain a robust thermo-mechanical design. The end result of this effort is a single dump design, related to an existing tune-up dump at CEBAF [6] which has operated for a number of years, that we believe can perform reliably at 250 kW with beam rastering, and at 120 kW without rastering.

Table 1: Performance Requirements

Dump	Beam Power (Max.)	Beam Energy (Nominal)
	[kW]	[GeV]
DUMPBSY	250	4
DUMPS	120	4
DUMPH	120	4

1.1 Beam parameters

Due to the extremely small emittance of the electron beam, LCLS-II is capable of producing very small spots on the face of the dumps. While the design optics was chosen to avoid such small spots, tuning the beam, even at the upstream end of the accelerator, can cause wide variation in the beta functions at the dump and inadvertently cause a small spot size. Values for beam parameters at the dump faces under nominal and most extreme (minimum beam size) operation conditions are given Table 3. The minimum beam sizes listed shown for the DUMPBSY were obtained by purposely distorting the optics to minimize the overall beam spot [7]. The resulting BMAG [8] mis-match parameter was 5. A BMAG mis-match parameter of less than 2 is expected in practice. For the undulator dumps, the minimum was obtained by scaling the beta functions down by a factor of 10. The beam is not expected to be round, but for simplicity the geometric mean beam size σ_r is listed in the Table.

Table 2: Estimated average usage of LCLS-II high power dumps.

	MW h / y	h / y	kW average
DUMPS	135	5000	27
DUMPH	239	5000	48
BSYDUMP	450	5000	90

1.2 Dump usage

Dump usage refers to the average beam power on the dump, where the average is assumed to be taken over a long period time such as a year. The estimate of the dump usage is described in detail in [3], and the highlights are shown here in Table 2. It is assumed that the machine operates for 5000 hours per year with the remaining time used for shutdowns, maintenance, etc.

1.3 Power cycles

Beam power delivered to the undulators is expected to vary considerably during normal operation depending on experimenter's needs. A typical session might involve a very low power tune-up beam, with a sequence of steps up in power, followed by a sudden drop when access to the experiment is needed. To avoid coupling the beam for one undulator with the beam from another as the experimenters needs change, the linac beam is held constant and the beam

in excess of demand is sent to the DUMPBSY by the spreader/kicker. As a result, all three dumps are expected to see a number of cycles, some of which have beam power up to or near the rating of the dumps. Based on anticipated experimenter usage, the estimated number of cycles that come within 25% of the rated power in thirty years is 4000 [9].

2 Mechanical

The basic components of the dump are shown in Figure 1. An aluminum vacuum beam tube is welded to the aluminum Inner Core and the assembly is inserted into the Outer Core and welded at the up-beam end only. Cooling water is brought in through Dump Water Supply tubes to the down-beam end of the assembly and then flows up-beam concentrically around the Inner Core. Cooling fins (80) are machined into the solid Inner Core to provide enhanced heat transfer from the aluminum to the water. The geometry of the fin cooling structure is shown in Figure 2. The number and aspect ratio of the fins was optimized to increase the wetted surface area while maintaining adequate mechanical strength for handling and manufacture. Once installed in the outer body, the fins will only be in contact with water and will bear no external forces. Clearance between the outer diameter of the fins and the inner diameter of the shell is provided for a loose slip fit at maximum thermal expansion of the core.

Beam power is converted to radiation and is mostly absorbed in the Inner Core. A small fraction is absorbed in outer core and is easily cooled by the Dump Water. A layer of steel shielding is put around the region of most intense radiation to absorb most of the remaining radiation that would otherwise heat the steel shielding in the dump. See Section 3.12. It is cooled by contact with the Outer Core.

A steel end cap is bolted to the downstream end of the dump to absorb a small amount of beam power that would otherwise penetrate the aluminum core and escape along the beam axis. The bolts are tack welded to the steel end cap to assure they cannot loosen. The higher density of steel compared to aluminum effectively shortens the overall length of the dump.

A Burn Through Monitor (BTM) is encapsulated by the Steel End Cap. It consists of a empty sealed volume that is pressurized to 5 to 10 psig. If beam were to somehow burn through the entire Inner core and the BTM the pressure would drop and a pressure switch would cause a trip of the PPS system. This type of event is not expected to ever happen.

3 Temperature and Stress

Temperature and stress issues are described in this section in some detail. They are critical to the performance of the dumps at high power.

3.1 Beam heating

Energy deposition by the beam was studied in [10, 11] for beam energy ranging from 2 to 8 GeV and for raster radius ranging from zero to 3 cm. FLUKA [12] was used to generate the dose maps which were then transferred to the thermal analysis program FHeat3D [13, 14]. The same dose maps were also used as input to independent thermal and stress analyses using ANSYS and TEM3P. The results of these simulations are used in the discussion that follows.

3.2 Peak temperature

Calculated peak temperatures at the rated beam powers are given in the Table 4. The peak temperature generally occurs on the axis about 40 cm from the front face. The calculated peak temperatures were obtained by adding the average temperature increase of the dump water to the peak temperature in the aluminum inner core calculated in simulation. In simulations the bulk water temperature all along the dump is assumed to be 35 C and the continuous rise of water temperature as it flows along the inner core is neglected. Results from different simulations were averaged. Peak temperatures for all cases are well below the melting point of 660 C.

While beam parameters and the design of DUMPS and DUMPH are identical, they are connected in series in the cooling water system with DUMPH being

Table 3: Electron beam properties at the dump faces at nominal and extreme conditions.

		DUMPBSY	DUMPS	DUMPH
ϵ_n	μm	1.0	1.0	1.0
Power	kW	250	120	120
Energy	GeV	4	4	4
Nominal				
β_x	m	363	42	31
β_y	m	354	4	6
$\sqrt{\beta_x\beta_y}$	m	367	13	14
σ_r	μm	217	40	42
Extreme				
$\sqrt{\beta_x\beta_y}$	m	30	1.3	1.4
σ_r	μm	125	13	13

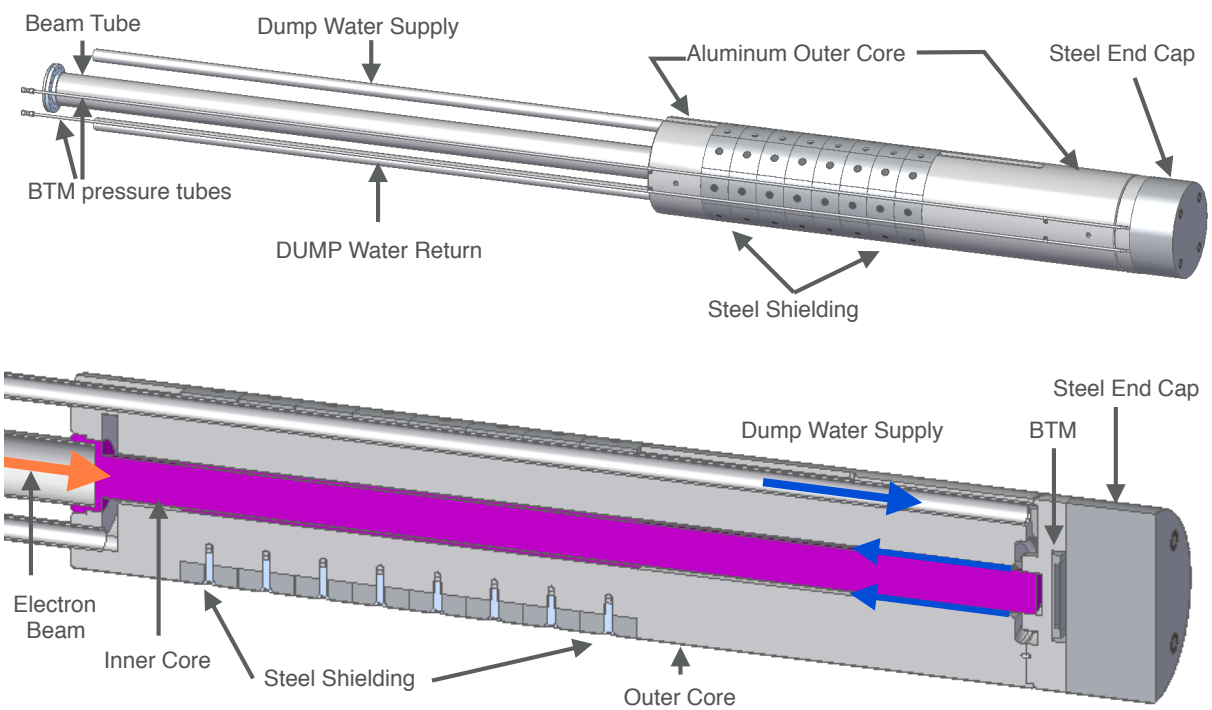

Figure 1: Dump subassembly.

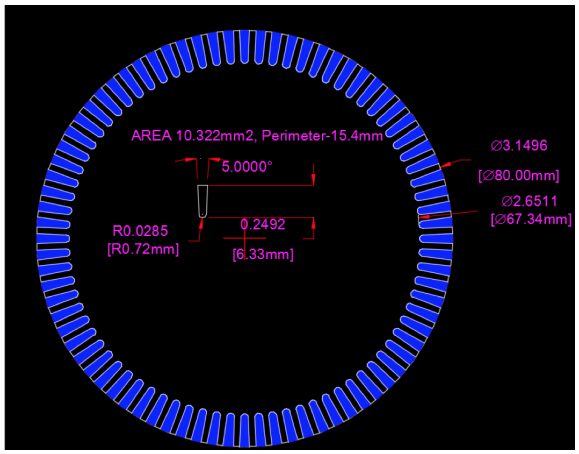

Figure 2: Section showing fin geometry.

Table 4: Calculated peak temperatures

Dump Name	Beam Energy [GeV]	Beam Power [kW]	Peak Temperature [C]
DUMPBSY	4	250	311
DUMPS	4	120	409
DUMPH	4	120	393
DUMPBSY	8	250	276

Table 5: Maximum thermal expansion.

		DUMPBSY 250 kW	DUMPS/DUMPH 120 kW
Length	mm	1.6	1.1
Radius	mm	0.14	0.09

cooled first. As a result DUMPH has slightly lower peak temperature than DUMPS. The values in the table reflect this arrangement.

The temperature distribution and profile calculated by simulation for the DUMPBSY is shown in Figure 3. This model includes 80 cooling fins that extend over the central 85 cm of the core. The graph shows the temperature profile along the center of the core where it reaches a peak of 556 K (283 C) for 4 GeV. The peak temperature is slightly lower at 8 GeV as the energy loss is spread out slightly and there is a small increase in escaped energy.

Analogous calculations were done for DUMPH and DUMPS and results are shown in Figure 4. In this non-rastered case the temperature is more sharply peaked toward the axis.

3.3 Overall thermal expansion

Two of the same analysis programs used to calculate temperatures in the dump core were used to calculate the thermally induced expansion. Using a coefficient of expansion of $2.4 \times 10^5/C$ and Young's modulus of 68.9 GPa, and a Poisson ratio of 0.33, assuming no yielding, the calculated maximum expansion is given in Table 5. Slight yielding may occur during the first thermal cycle to maximum power, but the analysis programs assumed no yielding, so actual expansion will be slightly more than calculated here. Clearances and tolerances take linear expansion into account, and additional clearance was included to account for the possibility of some yielding.

3.4 Dump face heating

When the beam first enters the aluminum of the dump core at the dump face, before there is any

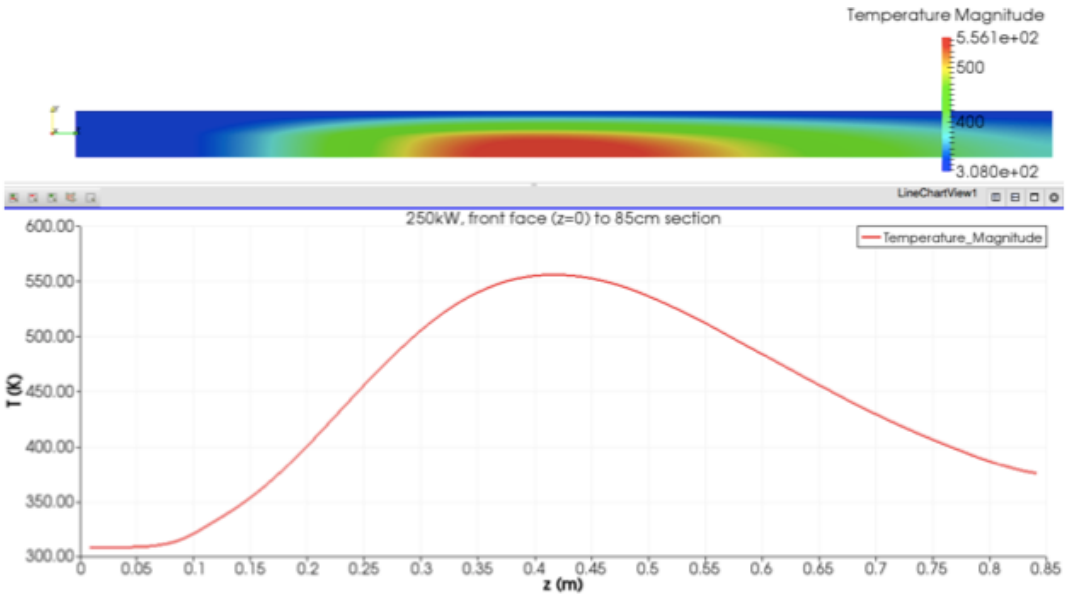

Figure 3: Calculated temperature radial and longitudinal temperature distribution for a beam of 250 kW, 4 GeV, and a 2 cm raster radius

shower development, it can be very small, (see Table 3). Electrons start to lose energy by generating bremsstrahlung radiation and through ionization of the aluminum atoms. Though the rate of energy loss from bremsstrahlung is far higher than from ionization, such energy is not absorbed near the dump face because the bremsstrahlung radiation is very penetrating and simply goes deep into the dump core before it is absorbed; leaving ionization as the only significant source of absorbed energy near the dump face [15]. Fortunately the ionization energy loss rate is so much lower than for bremsstrahlung that the net effect of the very small beam size on the peak temperature at the dump face is tolerable.

An estimate of the peak temperature at the dump face can be made using an analytic expression for heat flow under the assumption of cylindrical symmetry, no longitudinal heat flux, and constant absorbed power per unit length, dP_{abs}/dz. The minimum ionization loss rate for aluminum is 4.37 $MeV cm^{-1}$ [16]. If we employ the simplifying assumption that all the beam power is deposited uniformly within a radius equal to the gaussian beam size σ_r, then

$$\Delta T \approx \frac{dP_{abs}/dz}{2\pi K} \cdot ln \frac{R_{edge}}{\sigma_r},$$

where $R_{edge} = 4.0\ cm$ is the radius of the water cooling and $K = 167\ Wm^{-1}C^{-1}$ is the thermal conductivity, and ΔT is the temperature difference between the water cooled surface and the center of the beam as it enters the dump. For $\sigma_r = 10\ \mu m$ DUMPS and DUMPH beams, which are not rastered and limited to 120 kW, dP_{abs}/dz works out to 131 W/cm and $\Delta T \approx 103\ C$. There is virtually no film drop to the dump cooling water and with a 35 C water supply, the peak temperature at the face will only be about 138 C. Even if the beam size were reduced to 1 μm, the peak temperature on the face would only reach 167 C. For the rastered case the effective beam size is very large and the beam heating at the face can be neglected. See Section 4.1.

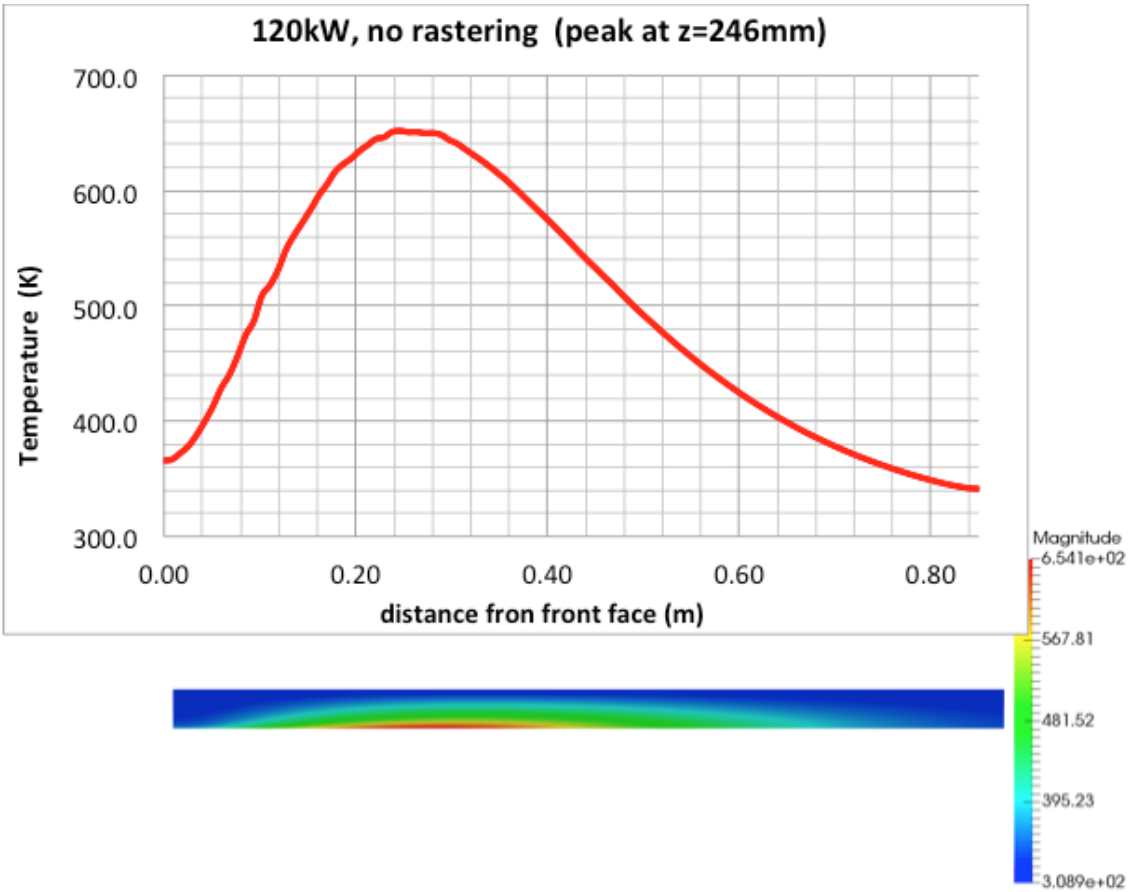

Figure 4: TEMP3P calculations of radial and longitudinal temperature distributions for a 120 kW, 4 GeV, beam with no rastering.

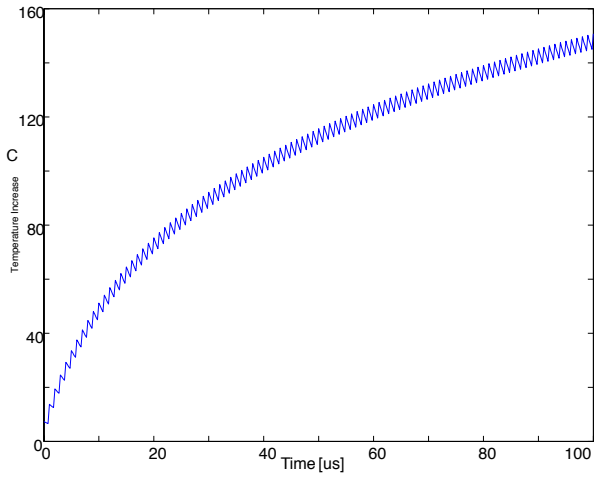

Figure 5: Transient temperature response in aluminum for 30 μm, 1 MW, 1 MHz, 4 GeV beam

3.5 Transients and bunch charge

A single bunch causes an essentially instantaneous transient temperature rise in the dump. If the charge is large enough, the amplitude of the temperature transient can be significant [17, 18]. However, for the range of bunch charge for which LCLS-II is expected to be operated the transient temperature rise is quite small.

Transient heating by the LCLS-II beam was studied in [19], [13], and by A. Lutman (unpublished). There are two primary features of interest:

- Instantaneous temperature rise due to a single bunch.
- Transient response to a sudden increase in beam power.

For the beam parameters of LCLS-II the transient response to a sudden application of high beam power is the more important feature. The highest bunch charge for operation, only 300 pC, produces a modest single bunch temperature rise in the dump as can be seen in Figure 5. The "teeth" on the temperature curve correspond to individual 300 pC bunch and are approximately 7 C high. On the other hand, it is not hard to come up with materials which, in the event of a sudden increase in LCLS-II beam power, would reach melting points in less than 1 ms. For the dumps however, with the relatively low Z and high thermal conductivity, the transient response is much more favorable.

3.6 Peak Stress

The design of the dump is such that as the temperature changes the inner core may expand freely from the single welded upstream end connection. This feature avoids build-up of differential thermal expansion between the core and the outer body. Nevertheless, within the core there can be large thermal stress as the hotter central axis tries to expand more than the outer surface where the water cooling is applied. In addition to the 'bulk' internal stress caused by the gross distribution of heating and cooling, there are small areas of enhanced 'local' stress associated with the fin structure. Table 6 lists calculated peak stress for various conditions and the yield and ultimate strength of the core material.

Stress was simulated independently using TEMP3D and ANSYS with good agreement. Particular attention was given to the von Mises stress. Zero pre-stress at room temperature was assumed. Typically as a function radial coordinate the von Mises stress goes through a minimum around 20 mm and then increases with radius. The highest von Mises bulk stress occur on axis where the stress is compressive. Material on-axis could yield but as long as the integrity of the material around it is intact, it cannot go anywhere. Near the outer radius of the inner core the material is in tension. For the 120 kW un-rastered case the peak von Mises stress is seen to reach 223 MPa in the groove between fins. See Figures 7, 8 and 9. For the 250 kW rastered case, the peak stress in the fin core reaches 249 MPa, and 330 MPa in the fin groove. See Figure 6. The longitudinal coordinate for this plot was chosen to coincide with the peak thermal flux and highest temperature. Simulations without fins show no local enhancement of stress at the outer boundary and peak von Mises stress considerably lower.

In the 250 kW rastered case, the calculations indicate the peak stress in the groove can reach slightly

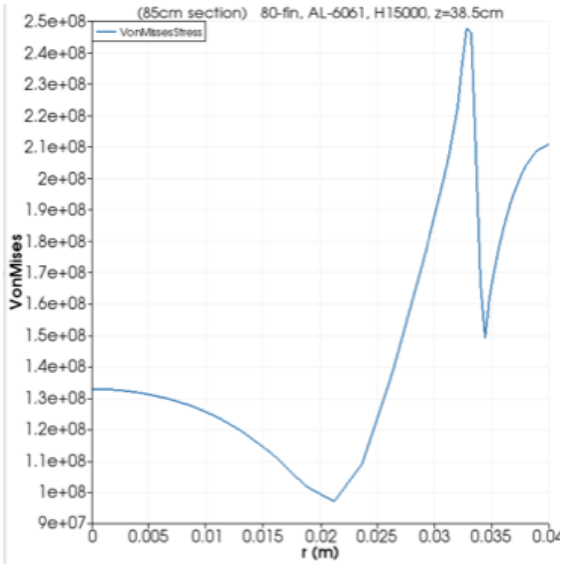

Figure 6: von Mises stress as a function of radial coordinate for a beam of 250 kW, 4 GeV, and a 2 cm raster radius, for the hottest longitudinal location

above the yield point and the material is in tension. Over a region of a few longitudinal centimeters we expect there will be yielding of the material on the first thermal cycle to maximum power. Nominally the stress on the first cycle would also be above the ultimate tensile strength. But the high stress point of the fin groove is longitudinally confined by adjacent cool material where stresses are well below the yield point, so breakage should not occur. The cyclic behavior of this case is discussed detail in Section 3.7.

Aluminum 6061 alloy was chosen over the 1100 series alloys because of the increased strength. Thermal stress scale inversely with thermal conductivity, indicating a higher stress for 6061 alloy compared with 1100 by a factor of approximately 220/167 = 1.3. However the yield strength of 6061 is greater than that of 1100 (H14) by a factor of 310/105 = 3.0, more than making up for the higher stress level.

It is possible material properties may change for aluminum that is subject to the most intense radiation dose and the high strength advantage conceivably could be lost. This is only of concern in the

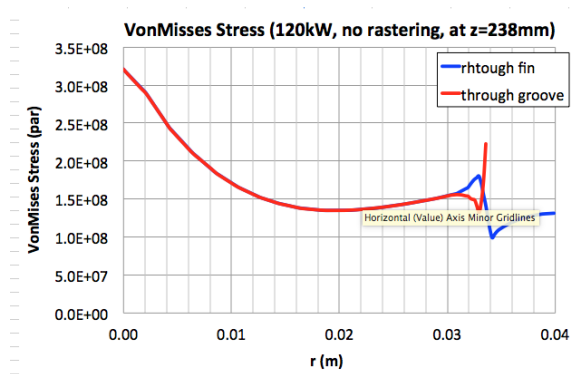

Figure 7: von Mises stress as a function of radial coordinate for a beam of 120 kW, 4 GeV, and a 2 cm raster radius, for the hottest longitudinal location.

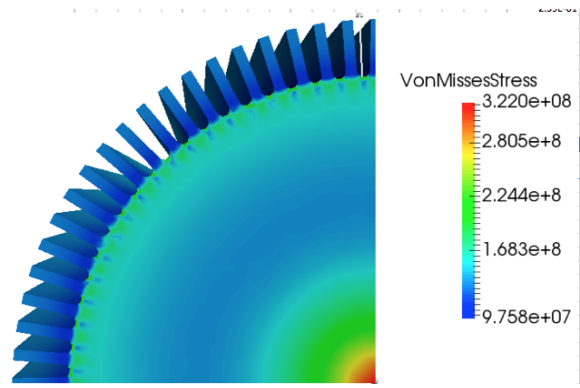

Figure 8: von Mises stress distribution over a slice of the inner core for a 120 kW, 4 GeV beam at for the hottest longitudinal location.

Table 6: Peak von Mises stress in the Inner Core

Location		120 kW no raster	250 kW 2 cm raster
Fin Groove	MPa	223	330
Fin Core	MPa	180	249
Central Core	MPa	322	132
Yield	MPa	276	276
Ultimate Tensile	MPa	310	310

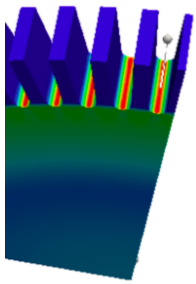

Figure 9: High (colored red) von Mises stress distribution in groove between fins.

central portion of the core. At the outer boundary, where the cooling water is applied, the radiation dose levels are not unusually high and the material can be expected to maintain its integrity. Stress related modification of the material near the axis is not expected to lead to any external or performance changes in the core since such material is confined.

Similarly the temper of the alloy will eventually be lost in places with the temperature above about 150 C. But such places are completely confined by cooler, largely un-radiated material, whose strength should not degrade.

3.7 Cyclic stress

Cyclic stress generated by thermal expansion is a concern in the inner core of the dump. Data for 6061 Aluminum shown in Figure 10 indicate that for stress ratio[1] of zero, the first failure was observed after 20,000 cycles to 275 MPa (40 ksi). Simulations of the 120 kW case show (see Table 6) peak stress on the central axis of 322 MPa, which is above the yield point. Evidently the material in that portion of the core will yield on first cycle to full power. Upon cool down that same material will end up in a compressive state so subsequent cycles will not get to as high peak tensile stress and the stress ratio will become slightly negative. Material surrounding material on the beam axis is not expected to yield because the stresses there are much lower, so the integrity of the core should be maintained.

A similar situation occurs at the base of the gap between the fins. Locally the stress is enhanced to as high as 330 MPa (48 ksi) in the 250 kW case. In this small region the aluminum will yield and then, upon cool down, it will be in a compressive state. Unlike the core, however, the base of the groove is not surrounded completely by material that is below the yield point so the integrity is not guaranteed. In the test data shown in Figure 10 a curve is fitted to data for zero stress ratio which intersects the peak fin stress between 10,000 and 20,000 cycles - uncomfortably close to the estimate number of lifetime high power cycles of 4000. However the test materials were subject to controlled amounts of axial tension and compression, the same for each cycle. As the materials yielded and lengthened the applied stress was artificially held constant. Subsequent cycles cause more and more elongation until failure. In the case of thermal stress, if the material yields the stress is relieved for future cycles. Consequently we expect far more cycles will be tolerated before a local failure of the fins than predicted in Figure 10. Failure, if it should occur, would probably take the form of the development of radial and longitudinal cracks originating in gap between the fins. Such cracks would not cause a performance problem unless they propagate enough to allow a fin to break off entirely. This is also unlikely since the upstream and downstream portions of the fins are in low stress regions.

3.8 Cooling radius

Heat transfer from the aluminum core to the cooling water was a critical factor in the optimization of the dump design. In establishing the cooling radius a balance had to be made between lower heat flux,(which lowers the film drop at the aluminum/water boundary) and higher temperature drop due to conduction in the aluminum core. In a cylinderically symmetric model of the dump which includes the film temperature drop and the conduction temperature drop, the radius at which the peak core temperature is mini-

[1] Stress ratio is the ratio of minimum stress to maximum stress in one cycle of loading. Tensile stresses are considered positive and compressive stresses negative [20].

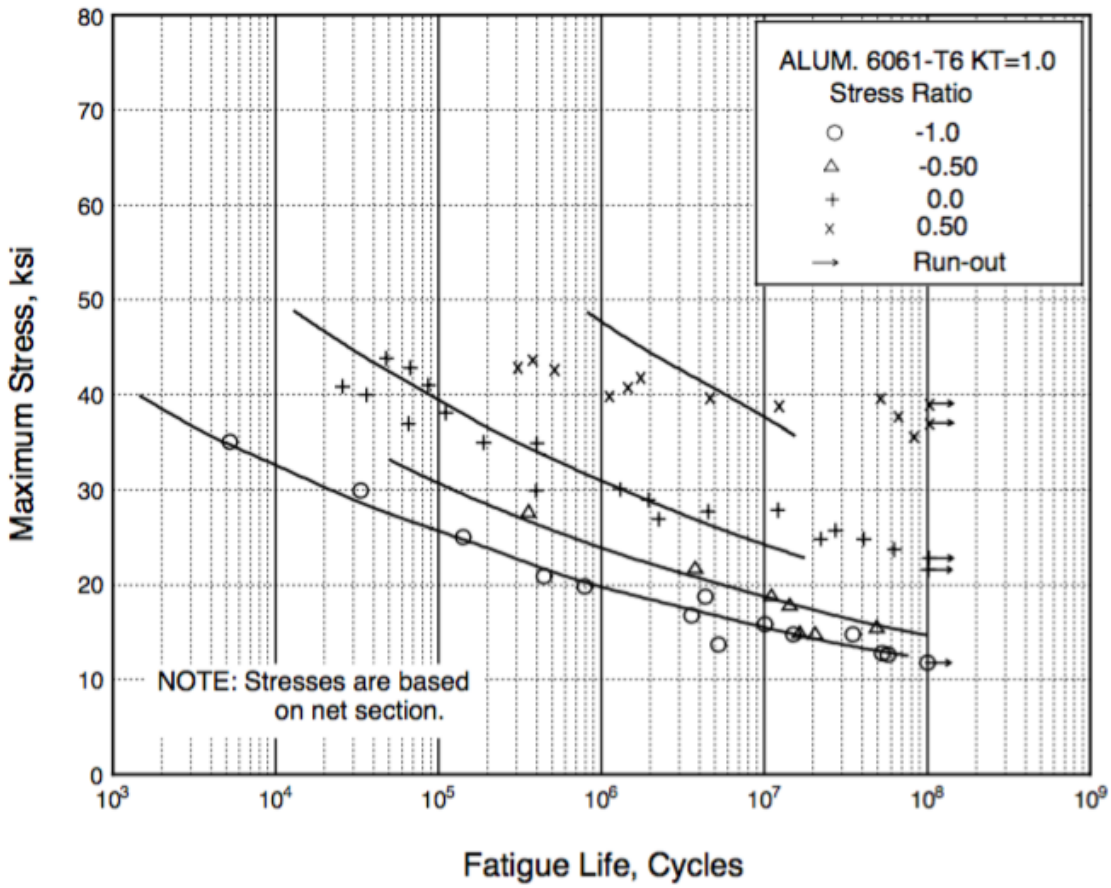

Figure 10: Fatigue life in cycles for 6061 Aluminum for various stress ratios [21].

mized is

$$R_{opt} = \frac{K}{h}$$

where K is the thermal conductivity of the core and h is the heat transfer coefficient at the water boundary. For example if $K = 167\ Wm^{-1}C^{-1}$ (6061 Al) and $h = 7000\ Wm^{-2}C^{-1}$ the optimum cooling radius is 24 mm. At such a small radius the radiation from the electron beam would highly activate the cooling water and that activity would be spread throughout the cooling system. To minimize such radiological problems we chose a larger cooling radius of 40 mm where irradiation of the cooling water is much less.

3.9 Heat transfer

High flow velocity reduces the film drop and lowers the core temperature, but too high flow velocity can cause excessive erosion. We based the design around a flow velocity limited to approximately 2.3 m/s. At a radius of 40 mm the peak heat flux at the water boundary for the 250 kW dump is estimated to be about 170 W/cm^2 assuming a purely annular geometry [22]. We employ cooling fins to increase the contact area of the water. The net effect is to reduce the heat flux by about a factor of five to around 34 W/cm^2. High resolution simulations show the temperature drop in the aluminum of the fins is negligible compared with the film drop, so the fins could be made thinner and the film drop reduced further. However, as the film drop is only 29 C, at most, there is little to be gained and it was felt that thicker fins are more robust.

A feature was added to the design of the core to enhance the transition from laminar to turbulent flow and thereby increase the heat transfer coefficient. Following [23] the development of turbulent flow follow the Reynolds number $Re_x = (x/2.7) \times Re_\infty$, where 2.7 is the hydraulic diameter in millimeters of the cooling fin channel, $Re_\infty \approx 6000$ is the Reynolds number for fully developed flow, and x is the distance along the flow channel from the start. The transition from laminar to turbulent flow has been measured to be in the range of $Re_x = 8 \times 10^4$ to 5×10^6 depending on the roughness of the flow channel and the initial state of the flow. This leads to a range of distance to develop turbulent flow in the fin channel of 36 to 2250 mm. To ensure that the flow is developed early on we added a special feature at the beginning of the fin channel that forces the water to develop transverse momentum to encourage turbulent eddy development.

Table 7: Cooling fin parameters.

Number of fins		80
Fin height	mm	6.33
Fin width	mm	1.212
Fin fillet radius	mm	0.72
Bare core radius	cm	3.367

Table 8: Selected heat transfer parameters.

Common		
Flow speed	m/s	2.3
Reynolds number		6088
Nusselt number		57
Heat transfer coefficient	$\frac{W}{m^2C}$	12794
DUMPBSY 250 kW		
Film drop	C	29
Wall peak temperature	C	96
DUMPS/DUMPH 120 kW		
Film drop	C	14
Wall peak temperature	C	72/57

3.10 Cooling sensitivities to mechanical tolerances

The fit or clearance between the inner and outer core can have an effect on the hydraulics and cooling. If the fit is very loose then for a fixed water volume flow rate the flow velocity at the heated surfaces will decrease and the film drop will increase. The pressure drop along the fins, ΔP_{fin} , will also decrease. The sensitivities of the some hydraulic parameters were calculated for the nominal and maximum clearances specified. Nominal clearance is defined to be at maximum material conditions. It represents the closest

Table 9: Hydraulic sensitivities to inner core fit.

		Nominal	Loosest	Loosest
Flow	gpm	30.0	30.0	**37.8**
Speed	fps	7.0	**6**	**7.6**
ΔP_{fin}	psi	6.7	**4.6**	6.7
Film drop	C	13	**14**	**12**

fit of the inner and outer cores (without taking into account thermal expansion during operation) and is a diametrical clearance of about 0.6% of the diameter. The results are tabulated in Table 9. Nominal values are listed normal font, and bold font highlights the values that change as result of the fit. The most obvious affect of the fit is on the fin pressure drop, which will be almost 2 psi lower than nominal for the loosest fit if the flow rate is held at 30 gpm. In this constant-flow-rate case, the change in the film drop due to the reduction in flow velocity cause by the loose fit is only about 1 C. If instead the pressure drop is held constant, the flow rate for the loosest fit will increase from 30 to 37.8 gpm.

If the fit is too tight there are two possible consequences; the parts won't go together, or when the dump is operated at high power, the inner core will thermally expand until it reaches the outer core diameter and bind with it. In the former, the inner core could be re-machined to a slightly smaller diameter. Of course it would be important not to jam the parts together with such force that they cannot be pulled apart. In the latter case there is some risk if the inner core binds up with the outer core that a portion of the fins will be radially compressed and could yield or conceivably break. As mentioned in Section 3.3 the radial thermal expansion is up to 0.14 mm or less, depending z-location and power level. That expansion uses up about half of the clearance at maximum material condition. This expansion only affects the inner core as the outer core has little heat generation in it.

3.11 Steel end cap

For a raster radius of 2 cm and a beam energy of 4 GeV the steel end cap absorbs about 0.35% of the beam power, which is 875 W for a beam of 250 kW. For a beam energy of 8 GeV the steel end cap would absorb about 0.602%, or 1.5 kW from a 250 kW beam. These powers were actually calculated for a copper end cap of the same dimensions [11], but are sufficiently accurate for our purposes.

Heat absorbed in the 30 cm diameter steel end cap is transferred to the water-cooled aluminum core by conduction with a nominal contact area of about 700 cm^2. For a 4 GeV beam running at 250 kW the total heat load from the cap is 875 W and the nominal heat flux is 1.25 W/cm^2. The end cap is bolted to the aluminum core, so the issues of thermal resistance of the contact and differential expansion are worth exploring.

A safe upper limit of the effective contact resistance can be made by assuming heat conduction from the steel end cap to the aluminum core is only through an air gap with a thickness roughly equal to the flatness tolerance of mating surfaces. In reality, while bolt forces provide metal to metal contact over an area much smaller than the nominal contact area, they also should reduce the size of air gap by causing the parts to conform to each other's shape. If we assume the flatness tolerance is sufficiently tight that the effective air gap is 0.1 mm (0.004 inch) and use the thermal conductivity of dry air $K_{air} = 0.0263\ Wm^{-1}K^{-1}$ (no convection) for the thermal resistance, then the calculated upper limit on the temperature drop for across the gap would be 47 C for a 250 kW, 4 GeV beam. The temperature of the dump body should be close to the water cooling inlet temperature which is held to be less than 35 C for DUMPBSY and DUMPH and 41 C for DUMPS. The internal temperature drop within the steel end cap is estimated, based on the assumption of uniform heat deposition, to be only 20 C. Thus the hottest spot in the steel end cap is less than $47+35+20 = 102$ C. Similarly, for the corresponding 8 GeV beam where the cap absorbs about twice as much power it should not be possible for any part of it to get above 149 C. We judge it unlikely to suffer

degradation due to oxidation that can occur at very high temperature.

Differential expansion over the diameter of the steel end cap and the aluminum core would be less than of order$\sim$ 0.24 mm for 4 GeV, 250 kW beams and less than 0.42 mm for 8 GeV, 250 kW beams. Repeated cycling, over a long period of time, could conceivably lead to bolts loosening and even falling out, thereby allowing separation of the steel end cap from the cooled aluminum core. For this reason the bolts are tack welded to the steel end cap after they are tightened.

3.12 Steel sleeve

The design includes a 75 cm long section of concentrically attached steel sleeve plates bolted to the cooled outer core of the dump to capture more beam energy than would have been captured with a purely aluminum structure. This was done to reduce the heat load on the surrounding shielding. See Section 3.13. This sleeve is cooled by direct contact with the aluminum outer core. As in the case of the steel end cap, issues of issues of thermal resistance of the contact and differential expansion are given careful consideration. In this case the maximum power the sleeve will absorb is about 5 kW and the contact area of the sleeve is about 7000 cm^2 — roughly ten times more than the contact area of steel end cap. The maximum average heat flux is about 0.7 W/cm^2 which is about one-half that of the steel end cap. Scaling from the steel end cap result, all other things being equal, at maximum power we should expect the temperature of the contacting surface of the sleeve to be an average of no more than about 25 C above that of the aluminum outer core. The temperature difference could lead to a differential thermal expansion over the length of the sleeve between the outer core and the sleeve of between 0.1 and 0.2 mm. The sleeve is made of many small pieces each secured with a single bolt in the center to allow for this expansion. In addition, the bolts are tack welded to the sleeve to prevent loosening.

3.13 Shielding heating

Not quite all the beam power is absorbed in the dump and carried off by cooling water. A fraction of the power is converted to radiation which escapes the dump and is essentially entirely absorbed in the steel and concrete shielding surrounding the dump. The escaped power will heat the adjacent shielding.

To reduce the escaped power to a level below a rule-of-thumb value discussed below, a one inch thick steel sleeve surrounding the outer core of the dump in the region where the radiation is highest was included in the design. For a 250 kW beam, without the sleeve the escaped power would be about 8 kW [10] while with the sleeve it is about 3 kW.

To set the scale for the heating of the escaped radiation we calculate the thermal gradient due to a heat flux of 1 W/cm^2 in steel with a thermal conductivity of 50 $Wm^{-1}C^{-1}$. That is $dT/dx = 1 \times 10^4/50 = 200\ C/m$. As the thickness of the steel shielding is of order 1 meter we might expect the shielding to temperature near the dump to eventually reach of order 200 C for the heat flux of 1 W/cm^2. The figure 1 W/cm^2 has in the past been used as a rule-of-thumb for the limit on shielding heating (D. Walz, personal communication). We too adopt this rule.

The actual heat deposited will vary with position along the dump reaching a maximum about 45 cm from the front face and falling off rapidly before and after the maximum (see Figure 3). The peak power loss per meter for a 250 kW BSY dump is about 4270 W/cm [24]. If 3 kW out of 250 kW escapes, the peak power loss per meter that heats the shielding is approximately $4270 \times 3/250 = 51\ W/cm$, which for a radius of 15 cm is equivalent to a peak heat flux of $51/(2\pi \times 15) \approx 0.5\ W/cm^2$ — a factor of two below the rule-of-thumb value.

Questions that are not answered by instead using the rule-of-thumb are:

- How hot is too hot?
- What is the effective thermal conductivity of a pile of steel plates.
- What is the three dimensional flow of heat.

- What is the appropriate usage factor given the very low heating rate (of order 12 hours per degree C) and the resulting long time for the shielding temperature to get near the equilibrium temperature.

We assume the answers to these questions are benign.

4 Beam Position Control

Beam position control is vital to the safe operation of the dumps. For DUMPBSY to run above 120 kW the beam needs to constantly move in a prescribed way, while for the undulator dumps the beam needs to be maintained at a constant position to within a prescribed radial tolerance.

4.1 Rastered beam

The DUMPBSY may see continuous beam power up to 250 kW and would reach damaging temperatures and stress if the beam spot was not kept moving to spread out the heat. This motion of the beam on the face of the dump is called rastering. If the rastering were to fail, the dump could be damaged. For that reason the rastering magnet and the BPM systems are part of the BCS and subject to special protections. Rastering is not needed for the 120 kW DUMPH or DUMPS. Detailed requirements for the rastering system are given in [25] and recapitulated here.

Rastering is accomplished using deflecting magnets to move the beam, two BPMs to verify the motion, and a feedback system to maintain the central beam trajectory. The rastering magnets are located approximately 60 m upstream of the dump. There are no focussing magnets between the raster magnets and the dump, so from the rastering magnets to the dump the beam should travel in a more or less straight line, only affected by static magnetic fields such as the earth's field. Furthermore, with no focussing in between, a circular kick is needed to produce circular motion. A BPM located near the rastering magnets and a second BPM is located near the dump are used to monitor the beam position. The BCS will trip if the beam position near the dump deviates beyond

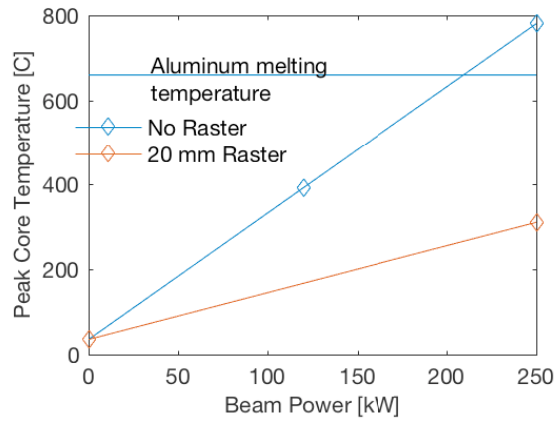

Figure 11: Dependence of stress in the Fin Core for rastered and non-rastered beams.

the allowed range given in Table 10. Orbit feedback is used to help keep this from happening. A BCS current sensor on the raster magnet power supply determines if the rastering magnets are powered at the proper strength, again tripping the BCS if the current deviates from the allowed range. The BPM near the dump should show the proper motion of the beam going around in a circle in the right location and the right diameter. The MPS will monitor this BPM and issue a fault if it should exceed allowed limits.

The limits on the rastering radius are determined on the high side by the need to avoid hitting the beam pipe wall with the beam halo and on the low side by the increase in stress that results when the radius is decreased. If the raster radius is reduced the stresses increase. Ultimately the stresses will increase by more than 50% for zero raster, in the linear approximation. See Figure 11 With about 25% increase they will exceed the ultimate tensile strength in the fin core. It seems reasonable to limit the increase in stress to about 5%, corresponding to 10% of the raster radius, i.e. 2 mm.

The choice of rastering frequency (see Table 10) is bounded on the low side by two factors:

- The need for the heat to evenly distribute around the rastering circle before it diffuses to the cool-

ing channels.

- The needs for the beam spot to move a distance greater than the diffused heat from the previous bunch so as to avoid thermal 'pile-up'.

It turns out that the second factor is the determining one.

The time scale Δt for heat to diffuse the distance and distance ΔL is $\Delta L^2/D$, where D is the diffusion constant which for 6061 aluminum alloy is about $6.9\times10^{-5}\ m^2/s$ [15]. The circular raster path is about 20 mm from the cooling channel, so the characteristic diffusion time is $\Delta t = 0.02^2/6.9 \times 10^{-5} \approx 6\ s$. The raster period must be much shorter than this characteristic time if the heat is to be spread out by the time it reaches the cooling channel.

The distance heat diffuses in the time between bunches depends on the repetition rate. Following calculations in [15], for the highest repetition rate of 929 kHz and a rastering radius of 20 mm, the heat diffuses about 9 μm in the time interval between bunches, and the minimum rastering frequency that insures the spot has moved more than the heat has diffused is 311 Hz. This means that, roughly, for a 1 Hz rastering frequency and a 929 kHz repetition rate, the heat from about 300 pulses would pile up before it had a chance to diffuse away. Calculations have shown that for LCLS-II parameters the instantaneous temperature rise due to an individual bunch is around 7 C or less (see Figure 5 which used 4 GeV 269 pC bunches). Clearly a 1 Hz rastering frequency would lead to unacceptably high transient temperatures.

In reality the pile up effect is diluted because there is substantial thermal diffusion occurring. Furthermore there is a limit on beam power which decreases the bunch charge, and therefore the instantaneous temperature rise, at high repetition rates where the diffusion time is shorter. For example, a 929 kHz beam cannot have 269 pC bunches since that would for 4 GeV amount to 1 MW and exceed the dump power rating by a factor of 4. Beams limited to 250 kW can have bunches up to 67 pC which will generate only about 1.7 C instantaneous temperature rise.

Table 10: Rastering parameters

		Min	Nominal	Max
Radius	mm	18	20	22
Center	mm	0	0	2
Frequency	Hz	10	30	100

With this reasoning in mind, a 10 Hz rastering frequency would imply transient temperature rise up to roughly 30 C which is about 10% of the total maximum equilibrium temperature rise and is acceptable. A nominal 30 Hz rastering frequency would imply transient temperature rise up to of roughly 10 C . These values are included in Table 10.

On the high side, the rastering frequency limit is due to eddy current shielding by the vacuum chamber. If we require the skin depth to be 10 mm or more, so that there would be relatively little shielding in the few millimeter thick vacuum chamber wall, then for an aluminum chamber the frequency would have to be less than about 100 Hz (skin depth is about 8 mm). For stainless steel chambers the frequency can be higher by roughly a factor of 5.

Specifications for rastering magnets are not yet defined. One possible arrangement consists of three conventional corrector magnets, arranged sequentially with a 60 degree rotation (roll) between adjacent magnets. A single conventional three-phase motor controller can then be used to power the magnets with a different phase for each magnet. This arrangement takes advantage of the reliability and stability of the three phase power of the grid. In principle two correctors with two power supplies 90 degrees out of phase could produce the required circular motion, but amplitude, phase, and frequency of the supplies would have to be tightly controlled. With a three-phase arrangement, only the amplitude needs control. A third possibility is to make one sextupole magnet and wire the poles as three pairs of dipoles. This is the arrangement used at CEBAF (C. Sinclair, personal communication).

4.2 Non-rastered beam

Deviation of a non-rastered beam from the dump center has the same types of hazards that are detailed for deviation of a rastered beam if the raster radius is too large. Tolerance on the maximum radial deviation for a non-rastered beam is chosen based on the one of the same criteria as is used for rastered beam, namely that irradiation of the cooling water does increase more than a factor of two. This occurs when the rastered beam is more than 22 mm from the center, so 22 mm is the tolerance on the relative radial position of the non-rastered beam with respect to the dump center

5 Cooling System

Requirements for the Cooling System, given in [1], provide diagnostics to detect fault conditions as well as a means of measuring beam power to calibrate the BCS ACMs. Schematics and tables of nominal and maximum values of the parameters taken from [1] are repeated here for reference in Figures 12 and 13, and Table 11. Discussion of the power limits of the cooling system can be found in Section 10.

Briefly, a closed-loop, nominally 30 gpm water flow is recirculated through a dump, a heat exchanger and an expansion tank. A small amount of the flow is bypassed to a resin tank and a filter to remove corrosion/erosion debris which can become radioactive. In the case of the undulator dumps, the dump water is connected in series. Flow is monitored for each loop. Pressure and temperature monitoring are provided at the input and output of each dump.

6 Operation and Maintenance

Operation of a dump consists of keeping the dump in a state where it is safe to put beam on it. Except for occasional maintenance the dump is continuously ready to accept beam and the cooling system monitored and running within parameters in the range given in [1].

Before high power beam can be put safely on the dump, a low power beam is established with feedbacks controlling the beam position so that it properly strikes the dump face. For the rastered DUMPBSY the beam parameters are given Table 10 and the topic is covered in detail in [25].

Ordinary maintenance consists primarily of occasional replacement of the resin tank cores and filters as well as flushing the system to remove some accumulated erosion corrosion products. The frequency needed is not well determined but is low, possibly less than once a year. It could be at intervals of months or years depending on water chemistry, scheduled downtimes, etc. Following an earthquake event, or from time to time when convenient, a check of the alignment of the dumps should be made. Repairs and/or replacement of pumps and diagnostics, and maintenance/repair to the ancillary Cooling Water system are to be expected, but only infrequently.

7 Installation and Removal

Installation and removal procedures are the same for DUMPS and DUMPH and are briefly described here. For the first installation the process starts with the removal of the existing LCLS shielding and dump. This exposes the concrete walls of the accelerator housing and the installation of the Core can proceed. Referring to Figure 14, the Girder Pedestals are located and installed, and bottom layers of shielding are placed and grouted. Since bottom shielding plate stack-up may not provide the proper profile due to rough housing floor flatness and shielding plate thickness tolerance accumulation, we use shims in the gap between the top of the bottom shielding and the base for the Core with iron.

The next step is to place the assembly of the Dump Subassembly, a wedge shaped steel piece that makes up for the 3.83 degree vertical angle of the beam, and shielding concentrically placed around the Beam Tube. See Figure 15. The Outer Core is equipped with tooling balls to facilitate proper position and orientation alignment. Three vertical adjustment screws provide three degrees of freedom (+/-Y, roll, and pitch). Three additional degrees of freedom (+/-X, +/-Z, and yaw) may be adjusted by temporary hydraulic or screw jacks. When the Outer Core is in the

Table 11: Diagnostics and various values. See [1] for details.

Undulator Dumps	Symbol	Units	Nominal 27+48 kW	Max Power 2×120 kW
Dump Water flow	F_U	gpm	30	30
DUMPH water inlet temperature	$T_{H\ in}$	C	35	35
DUMPH water outlet temperature	$T_{H\ out}$	C	39	41
DUMPS water inlet temperature	$T_{S\ in}$	C	39	41
DUMPS water outlet temperature	$T_{S\ out}$	C	43	56
Pressure drop across combined dumps	$P_{H\ in} - P_{S\ out}$	psi	23	23
Pressure at Pump inlet	$P_{P\ U\ in}$	psig	30	30
Pressure at Pump outlet	$P_{P\ U\ out}$	psig	53	53
Pressure at DUMPH inlet	$P_{H\ in}$	psig	53	53
Pressure at DUMPH outlet	$P_{H\ out}$	psig	42	42
Pressure at DUMPS inlet	P_{S_in}	psig	42	42
Pressure at DUMPS outlet	$P_{S\ out}$	psig	30	30
Cooling water flow	$F_{C\ U}$	gpm	-	-
Pressure at HX cooling water outlet	$P_{C\ U}$	psig	100	100
Pressure advantage of Cooling Water	$\Delta P_{H\ U}$	psig	70	70
Cooling water HX inlet temperature	$T_{C\ U\ in}$	C	-	-
Cooling water HX outlet temperature	$T_{C\ U\ out}$	C	-	-
Resin system flow	$F_{R\ U}$	gpm	1	1
Expansion tank level	L_U	%	56	56
BSY Dump	**Symbol**	**Units**	**Nominal 90 kW**	**Max Power 250 kW**
Dump water flow	F_B	gpm	30	30
DUMPBSY water inlet temperature	$T_{B\ in}$	C	35	35
DUMPBSY water outlet temperature	$T_{B\ out}$	C	46	67
Pressure drop across DUMPBSY		psi	12	12
Pressure at Pump input	$P_{P\ B\ in}$	psig	30	30
Pressure at Pump output	$P_{P\ B\ out}$	psig	42	42
Pressure at DUMPBSY input	$P_{B\ in}$	psig	42	42
Pressure at DUMPBSY output	$P_{B\ out}$	psig	30	30
Cooling water flow	$F_{C\ B}$	gpm	-	-
Pressure at HX cooling water output	$P_{C\ B}$	psig	100	100
Pressure advantage of Cooling Water	$\Delta P_{H\ B}$	psig	70	70
Cooling water HX inlet temperature	$T_{C\ B\ in}$	C	-	-
Cooling water HX outlet temperature	$T_{C\ B\ out}$	C	-	-
Resin system flow	$F_{R\ B}$	gpm	1	1
Expansion tank level	L_B	%	56	56

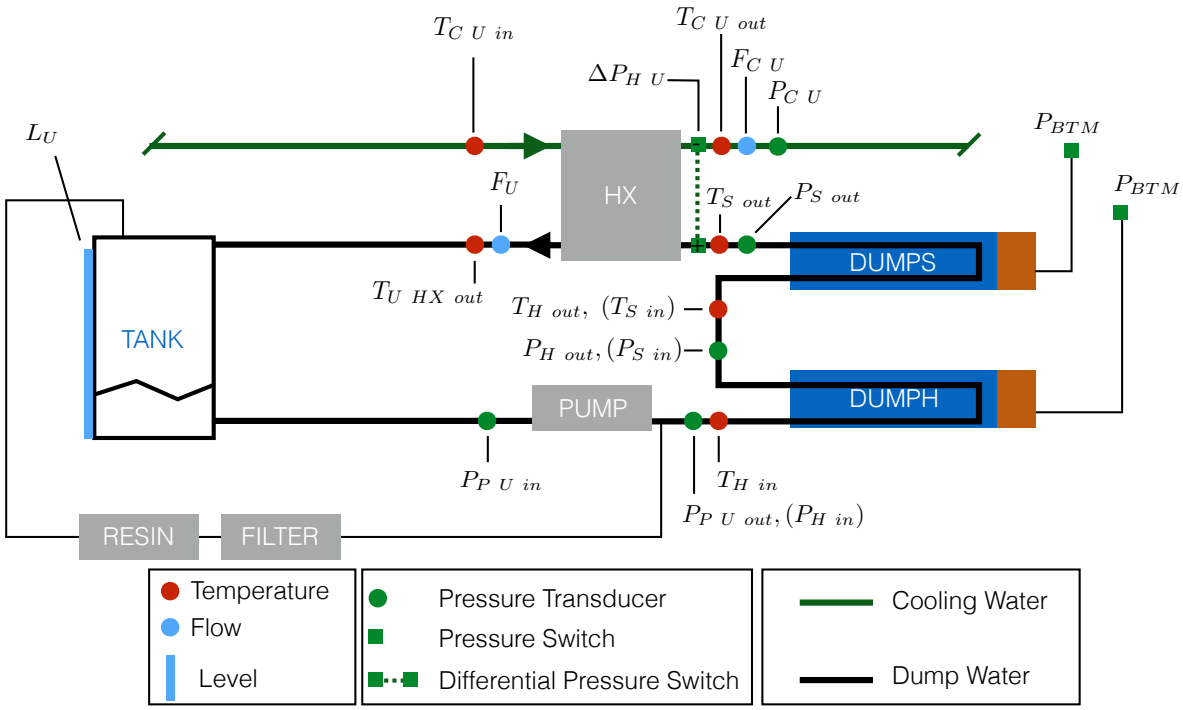

Figure 12: Schematic of undulator beam dump cooling system with diagnostics.

proper position, we weld the Wedge to the shim plates to make a solid monolith to protect the structure from motion during seismic event. Once the Outer Core is in the proper position and the secured, the shims are welded in place and the rest of the shielding is placed and grouted.

The procedure to remove the Core is somewhat different because of the high radiation levels present. The procedure avoids direct exposure to radiation from the Core by setting up a shielded box called a "coffin" into which the Core is pulled by a cable. See Figure 16. The Coffin is needed because steel shielding around the Core will become too activated. Fresh iron and lead is needed to shield the Core.

First there must be a wait period after the last beam for a time that is designated by Radiation Physics. After that we cut off the vacuum, cooling water and nitrogen lines using a hydraulic cutter, and then remove the Diagnostic Table. A Core Enclosure (Coffin) is then put in place of the Diagnostic Table on top of the Girder Pedestals. The Coffin is opened by pulling on a heavy steel vertical sliding door and a cable is attached to the eye bolt on the Outer Core. The shielded dump assembly is supported by four track bearings that allow motion parallel to the beamline. A winch then pulls the shielded dump assembly into the Coffin. Once that is done the Coffin door is closed and the Core plus Coffin assembly can be lifted and removed.

To install a replacement Dump, the winch system is set up on top of the Diagnostic Table and the gravity is used to roll the new Core into the position of the old Core.

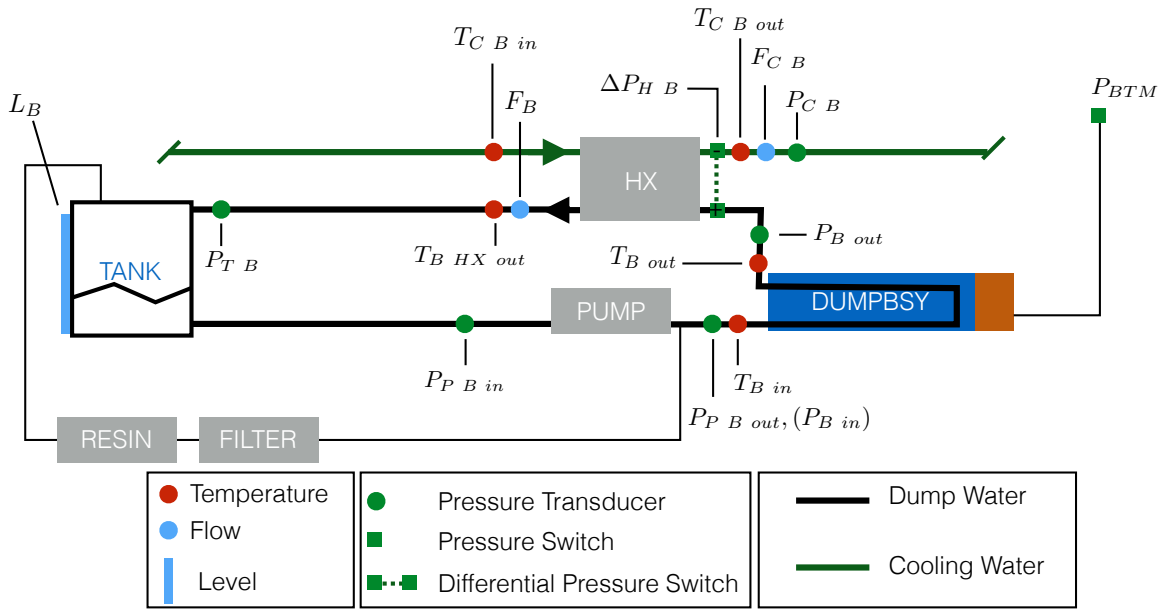

Figure 13: Schematic of DUMPBSY cooling system with diagnostics.

8 Safety

The beam dumps are components of the Beam Containment System (BCS), which is a automated beam safety system that ensures the electron beams do not escape their intended channels nor exceed allowed beam powers. This system monitors the beam power and trips off the beam if the power exceeds the allowed beam power for that location. The allowed beam power can never be more than the dump power rating.

The dump design is deliberately conservative. It is inspired by the design of dumps operated at CEBAF for over two decades [6]. The peak temperatures are far from the melting point, and there are multiple indicators of cooling faults. In addition, a burn-through monitor is located on the downstream end of the dump. In the very unlikely event the beam melts its way through two meters of aluminum and steel, when it hits the BTM it is expected to burn through and cause a PPS fault to turn off the beams.

The expected lifetime of the dumps is set by the lifetime of the facility. That is, there are no reasons to expect the dumps to wear out or fail prior to the end of use of the facility. Considerable thought and planning has gone into the design to minimize personnel exposure when removing the shielding and radioactive dumps when the facility needs to be decommissioned, or in the very unlikely event of a dump failure.

9 Radiation

All three dumps are very well shielded to prevent prompt radiation from reach occupied areas and for residual radiation following a one hour cool-down period. The shielding is also designed to limit the production of tritium in the adjacent soil to below the EPA detection limit [24]. Prompt radiation inside the accelerator housing (but outside the dump local shielding) which might affect electronic equipment is estimated to be moderate. Radiological issues connected with the dump cooling water are discussed in

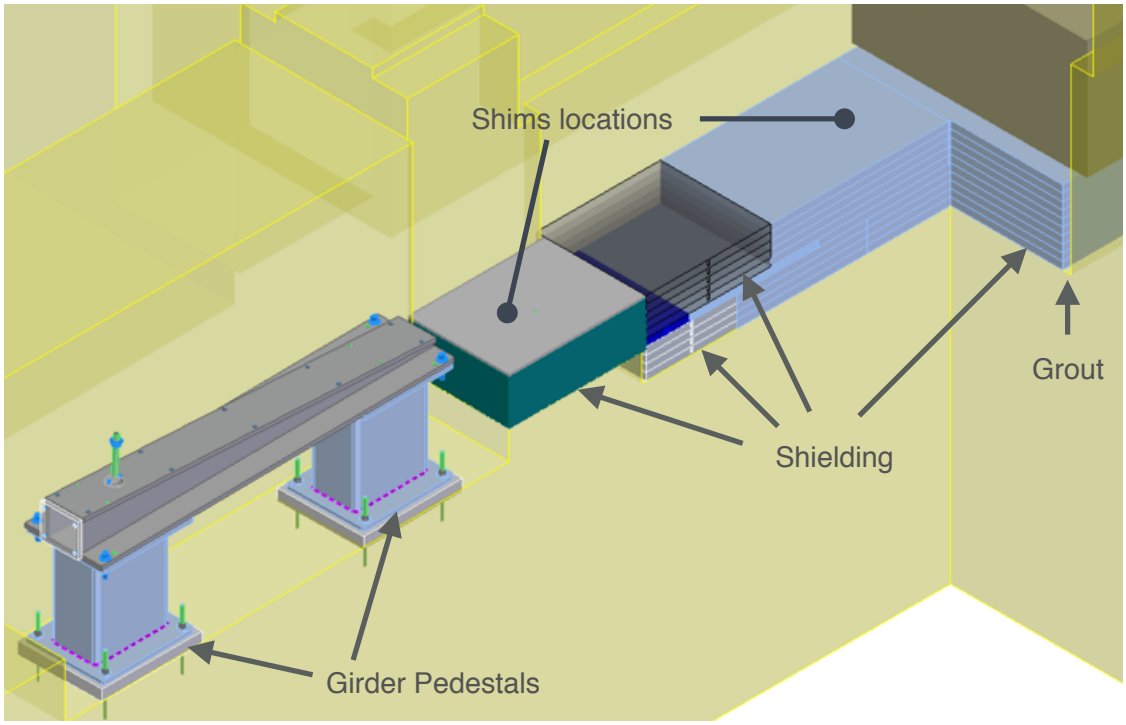

Figure 14: Configuration just before a shielded dump assembly is placed.

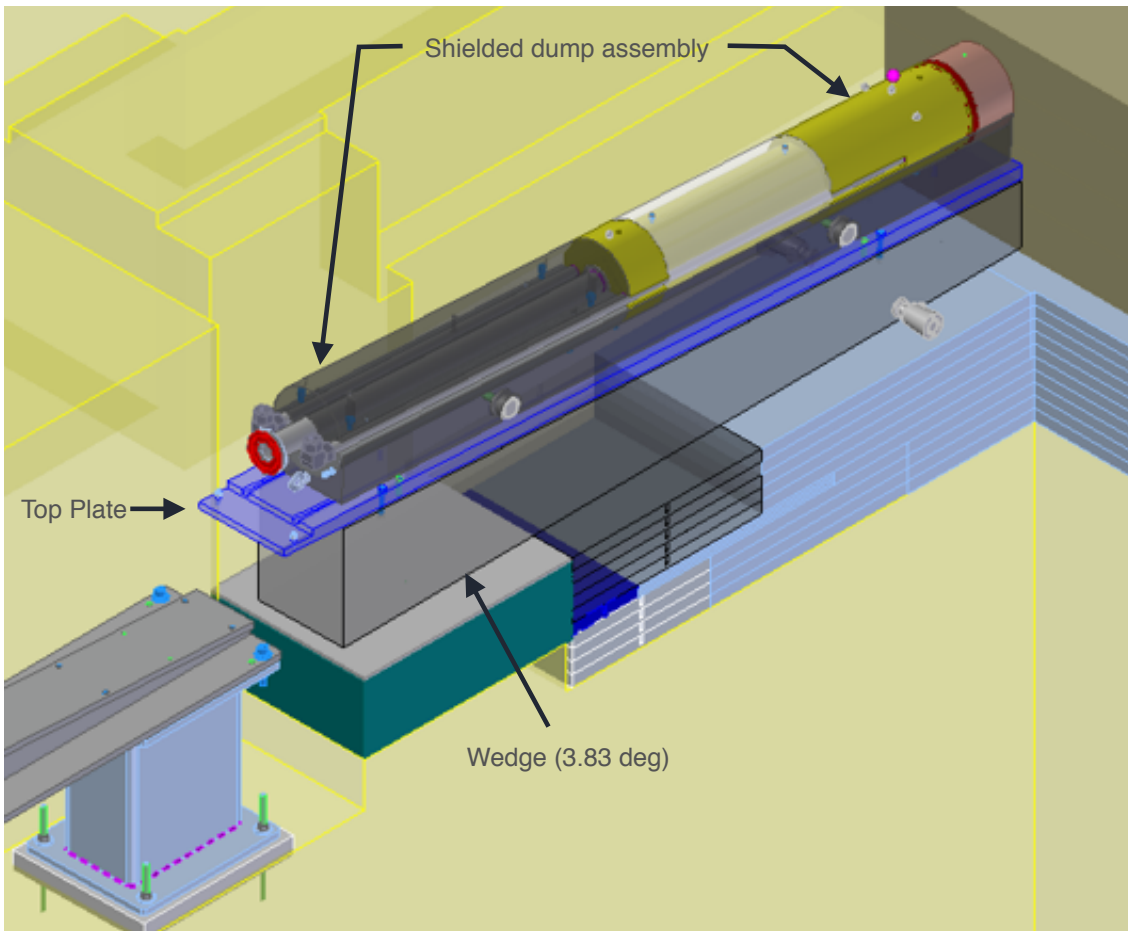

Figure 15: Configuration just after a shielded dump assembly is placed.

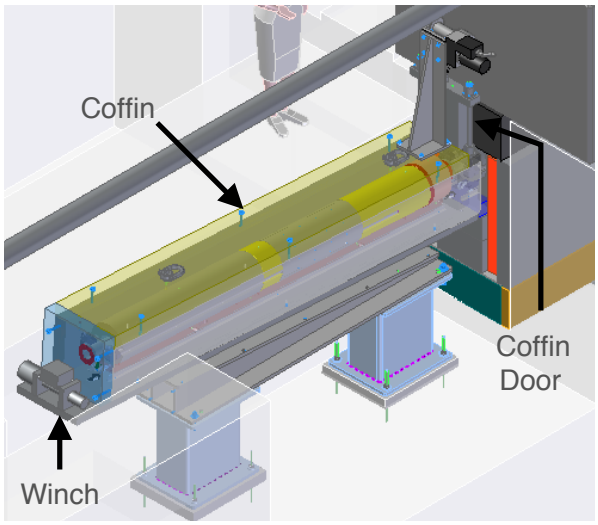

Figure 16: Radioactive core inside the "coffin" of fresh steel and lead.

[26].

If the dump is required to run up to 8 GeV some changes to the shielding may be necessary to obtain the same level of radiation in the soil as for 4 GeV. Possibilities are discussed in [27].

10 Performance Margins and Rating

The dumps are designed to safely operate up to the beam power and energy given in Table 1, and for usage factors given in Table 2. Testing to find the actual failure point is unfortunately not practical. In this section we discuss the estimated performance margins.

10.1 Melting

Estimated beam power required to reach the melting temperature in the inner core are listed in Table 12. These are obtained from the calculated temperatures at the design power limit given in Table 4 using the following:

$$\hat{T} = T_{inlet} + \frac{\Delta T_{H_2O}}{2} + \Delta T_{core} + \Delta T_{film}$$

where $\hat{T}$ is the peak temperature in the aluminum core, T_{inlet} is the temperature of the cooling water supply, ΔT_{H_2O} is the temperature rise across the cooling water, ΔT_{core} is the temperature drop across the aluminum core, and ΔT_{film} is the temperature drop from the aluminum to the cooling across the boundary layer. All of the quantities on the right hand side except for T_{inlet}, which is fixed, are proportional to the beam power, assuming the flow rate is held constant. Because the thermal conductivity is expected to be almost independent of temperature, a linear extrapolation of the core temperature drop as a function of power is reasonably accurate. Failure is assumed to occur when $\hat{T}$ reaches the melting temperature, 660 C. Such melting could eventually lead to beam penetration of the dump as was seen in the high power destructive beam tests in [28].

Because the two dumps are connected in series in the cooling circuit DUMPS fails at a lower power than DUMPH. In Table 12 the Failure Power for DUMPS was calculated with the assumption that DUMPH was simultaneously at its Failure Power. If DUMPH was limited to 120 kW the Failure Power for DUMPS would be about 265 kW.

Table 12: Dump beam power ratings and performance margins

	Rated Power [kW]	Failure Power [kW]	Failure Mode [kW]
DUMPBSY	250	565	melting
DUMPS	120	200	melting
DUMPH	120	270	melting

10.2 Number of cycles

What beam power would it take to cause a stress-related failure assuming the aluminum does not first

melt and that heat is removed normally by the water cooling system? What would such a failure look like?

It is enlightening to note that thermal expansion is much smaller than elongation required for breakage of aluminum. Overall thermal expansion, given Table 5, converted to strain yields overall strain for the 250 kW case of 0.35% radially and about 0.1% longitudinally. This can be compared with elongation at break in the range of 12-17% [29]. It would take beam power in the 10 MW range for single thermal cycle could rip the aluminum apart via thermal expansion. Melting failure would certainly precede such an event, and such high beam power is not possible at LCLS-II. However, failure from a number excessive power cycles is possible.

As noted in Section 3.7 thermal expansion does not produce the same stress each cycle once the material has started to yield. For the mild yielding expected at the rated maximum beam power, yielding in tension causes compressive stress for zero beam power that is just sufficient to prevent yielding on the next cycle. In this case there should be no limit to the number of cycles.

If the beam power is far above the rated beam power, it is possible the expansion is so large that the residual compressive stress is at the yield point, the stress ratio is -1.0 and material continues to flow radially each cycle. This might lead to failure in the form of the fin groove filling in with material. To get to this state the beam power would have to be at least high enough to produce twice the theoretical yield stress in the fin groove, which for the rastered 250 kW case implies a beam power greater than or equal to $2 \times 250 \times 276/330 = 418\ kW$. If the beam power were raised to 418 kW, after one cycle the stress ratio would be -1.0 and each cycle the material would reach the yield point in tension and in compression. According to data in Figure 10 we might expect the fin groove to lose integrity after around 1000 such cycles of the rastered beam on DUMPBSY. For the un-rastered beam, a similar scaling calculation leads the beam power of $2 \times 120 \times 276/223 = 297\ kW$ that would be sufficient cause fin groove failure after around 1000 such cycles.

10.3 Heat flux and burnout

Though the peak wall temperature is near the saturation temperature the system is very far from the critical heat flux needed for burnout. The peak heat transfer coefficient is at least two orders of magnet less than the critical heat flux under the most conservative assumptions. Using tables provided in [30], assuming no vapor phase in the cooling water (zero Quality), 30 gpm, and conservatively assuming no sub-cooling and atmospheric pressure, the critical heat flux is estimated to be about 18 times higher than the maximum heat flux when operating at 250 kW. Under such conditions even a trickle flow that is completely vaporized would provide enough cooling to avoid burnout.

10.4 Bunch charge

The temperature difference between the melting point, 660 C, and the highest equilibrium temperature for maximum power operation, 409 C, is 251 C. We posit that, even under maximum average operation, we can safely allow a bunch charge up to that which corresponds to 10% of that difference, 25 C. Scaling from the 300 pC case, described in Section 3.5, the maximum allowable charge is $300\ pC \times 25/7 \approx 1\ nC$. Much higher charges could be allowed, but not at the maximum average power.

10.5 Power ratings

The purpose of stating a dump power rating is to provide a convenient, clearly understandable, value for the beam power below which safe performance can be assuredly maintained. It is understood that operation above the rating might be possible, but may involve dump failure risks. The dividing line between assured performance and failure risk is not sharp. Because power related failures can involve considerable facility down-time and risk radiation exposure to those involved in replacing dumps it is better to somewhat bias the rated power toward assured performance and away from risk of failure.

The beam power ratings for high power operation are given Table 12. They take into account the ex-

tensive modeling and analysis on beams with energy from 2 to 8 GeV, much of which is described in this paper. The Cu linac will be able to generate higher energy beams, perhaps as high as 17 GeV. The dumps can easily accommodate such high energy beams. They are very low power, usually less than 1 kW and BCS limited to less than 5 kW. The inner core of the dumps is about 1.6 m long, which is about 18 radiation lengths. We don't expect much difference in the stopping ability of the dumps for beams up to 17 GeV compared with that of 4 GeV beams. A 17 GeV electron will be about 6 GeV after about one radiation length, leaving 17 radiation lengths for attenuation of the shower. Thermally the higher energy spreads the heat out a bit more and increase the beam power performance margin slightly.

11 Failure Modes and Effects

An Failure Mode Effects Analysis (FMEA) process was undertaken to identify possible failure modes for the dump system, what the hazardous consequences might be, how such failure would or would not be detected, and what mitigation actions could be undertaken to reduce the likelihood of occurrence or severity of the consequences. The results of complete analysis is in the form of a spreadsheet. After filtering, 49 types of possible failure events are analysed. The types of failures are categorized into:

Cooling failures events which might cause the cooling system to not operate within it's design parameters,

Diagnostic failures events caused by diagnostic errors that might lead to non-operation or actual failures of dump systems components,

Core failures events which might lead to a burn-through of the core,

Alignment failures events which might lead to beam hitting the dump outside the design range,

Radiation failures events which might lead to higher than expected exposure,

Installation/Removal failures events that prevent planned installation or removal,

Other all other events that cause the dump to perform in a way it was not intended.

The most numerous types of failure events listed are for Cooling failures (18). They included a variety of leaks, obstructions, corrosion related problems, resin tank failures, mistakes in plumbing, cavitation, and more. In all cases some reasonable mitigation action is identified including making test welds, pressure and vacuum testing of all joints, locating filters downstream of the resin tanks and upstream of the dumps, and a number of maintenance actions.

Diagnostic failures listed include software errors and failure of diagnostic instruments, but mostly are concerned with damage to the BTM which could lead to a dump replacement. Special features are included in the design to protect the BTM and its lines.

Core failures, though felt to be highly unlikely, include melting through by the beam, the effect of bolt breakage, transmutation gas build-up and damage to the core by a mis-steered high power beam. In one case, transmutation gas build-up, there is no direct detection mechanism identified. But the consequence would be swelling and degradation of the cooling channels causing a failure of the cooling system which is well instrumented.

Alignment failures identified, which might be caused by an earthquake or even a loss of alignment data, could cause the beam to strike the dump too far from the center and generate excess radioactivity in the dump water and additional thermal stresses. Special alignment features and procedures are included as mitigation for these types of failures.

Only two Radiation failure modes are identified: one due to unexpected material composition and one due to corrosion. The mitigations are to verify material composition for the dump core and to add an anti-corrosion black-oxide coating to some shielding sleeve pieces.

Installation/removal failures generally might lead to additional exposure to personnel who have to fix the problems. There are four such failures listed.

The final category, Other failures, includes fire, flood, rastering failure, excess beam power, over-

focussing of the beam, quality control problems, and loss of operational information about how to run the dump.

It is likely that one or more significant earthquakes will occur during the service life of the dumps; smaller earthquakes being more frequent. The accelerator housing surrounding the Undulator Dumps is very robust with reinforced concrete walls, ceiling and floor that are many feet thick. The undulator dumps are mounted very securely to the steel shielding which is trapped by and grouted to the accelerator housing. Consequently the most probable scenario is that, following an earthquake, the dumps will not be damaged and it is only necessary to check the dump is still in the proper position. Additional verification of the integrity of cooling and vacuum systems (which are external to the shielding) will, of course, be needed as well. Position integrity is determined by observation of fiducials on the vacuum chamber that is welded to and extends from the outer dump core.

Corrosion at a modest level is expected, but not severe corrosion that would be associated with core decompostion or serious shielding contamination. Corrosion, and in particular corrosion in a high radiation environment, could conceivably limit the useful lifetime of the dumps. There is an historical account that warrants some optimism regarding corrosion of the wetted aluminum surfaces. At SLAC 600 to 800 kW beams were run on the SL10 collimator, which was installed in the mid-1960s and consists of an aluminum chamber containing aluminum spheres and water. The wall thickness in the 6061 aluminum modules from the vacuum interface to the cooling water is 1.25 mm. To date no failure has been observed of this system (D. Waltz, private communication, August 2016)

Corrosion of surfaces exposed to air and high radiation will likely oxidize. The AP9 dump at FNAL had to be replaced because of a water leak. Among other things, 'there was rust all over everything' which made containment issues more difficult (R. Lebeau, FNAL, private communication, April 2017). We are coating some steel pieces that see the highest radiation to reduce corrosion. Overfocussing of the beam is expected to occur on occasion during tuning at low beam power. All other listed events are not expected to occur during the lifetime of the facility.

Table 13: Time to begin melting for various worst case scenarios.

Event	Time	
Rastering is suddenly removed from the DUMPBSY running at 250 kW	2.0 - 4.1	s
A 1.2 MW beam is suddenly sent to DUMPBSY previously running at 250 kW	1.8 - 3.4	s
The cooling system stops while DUMPBSY is running at 250 kW	18 - 24	s
A 250 kW beam is suddenly sent to DUMPS or DUMPH previously running at 120 kW.	8.5 - 12.5	s
DUMPS or DUMPH is running at 120 kW and the cooling suddenly stops.	35 - 38	s

12 Time to Damage

Estimates of the time it takes for dump damage to occur in a few 'worst case' excess beam power failure scenarios have been made using the tools developed to study the transient heating of the dumps [10]. Note that 'damage' is assumed to occur when the aluminum core reaches the melting temperature. Burn-through times are much longer. The results are listed in Table 13. All times are substantially longer than a typical BCS response time.

References

[1] J. Welch, "Beam Dump Cooling Systems, and Diagnostics," Physics Requirements Document LCLSII-2.4-PR-0858-R0, SLAC, January 2017.

[2] T. Raubenheimer, "LCLS-II Parameters," Physics Requirements Document LCLSII-1.1-PR-0133-R3, SLAC, May 2016.

[3] J. Welch, "LCLS-II Electron Beam Loss and Maximum Credible Beam," Physics Requirements Document LCLSII-2.7-PR-0079-R1, SLAC, October 2015.

[4] L. Y. Nicolas, "Environmental and residual dose rate aspects associated to using BSY D10 as LCLS-II high power dump," Radiation Physics Note RP-14-08, SLAC, April 2014.

[5] L. Y. Nicolas, "Simulations of the radiological impact of having D10 as high power beam dump for LCLS-II inside the BSY muon shielding," Radiation Physics Note RP-15-06, SLAC, April 2015.

[6] M. Wiseman, C. K. Sinclair, R. Whitney, and R. Vetterlein, "High Power Electron Beam Dumps at CEBAF," *Conf. Proc.*, vol. C970512, p. 3761, 1997.

[7] Y. Nososchkov, "unknown." Slides from March 10, 2016, March 2016.

[8] F.-J. Decker, C. Adolphsen, W. J. Corbett, and P. Emma, "Dispersion and betatron matching into the linac," in *Particle Accelerator Conference*, vol. 2, pp. 905–907, IEEE, May 1991.

[9] J. Welch, "Estimated number of high power cycles on LCLS-II dumps." LCLS-II memorandum, November 2016.

[10] M. Santana-Leitner, "Energy deposition and heat transfer studies for LCLS-II CEBAF type dumps," SLAC Radiation Physics Note RP-16-10, SLAC, June 2016.

[11] M. Santana-Leitner, "Energy deposition and heat transfer studies for Oct-2016 version of LCLS-II CEBAF type dumps," SLAC Radiation Physics Note RP-16-25, SLAC, October 2016.

[12] A. Fasso, A. Ferrari, and P. Sala, "Electron-photon transport in FLUKA: Status," in *Proc. MonteCarlo 2000 Conference, Lisbon* (A. Kling, F. Barao, M. Nakagawa, L. Tavora, and P. Vaz, eds.), pp. 159–164, 2001.

[13] M. Santana-Leitner, "FHeat3D, a heat evolution plug-in for FLUKA monte carlo code: Example of use for LCLS-II BCS response time definition'," Radiation Physics Note RP-14-07, SLAC, April 2014.

[14] M. Santana-Leitner, "Benchmarks of FHeat3D heat evolution code," Radiation Physics Note RP-16-04, SLAC, February 2016.

[15] J. Welch, "LCLS-II BSY dump window and beam rastering," Tech Note LCLS-II-TN-16-02, SLAC, June 2016.

[16] Anonymous, "Review of particle properties," *Phys. Rev. D*, vol. 45, pp. S1–S574, Jun 1992.

[17] M. C. Ross, R. Iverson, K. Jobe, D. McCormick, P. Tenenbaum, and P. Raimondi, "Single pulse damage in copper," SLAC Pub SLAC-PUB-8605, SLAC, September 2000.

[18] M. Schmitz, "Description of the beam dump systems for the European XFEL," specification, DESY, December 2013. Revision 2.1.

[19] M. Santana-Leitner, "Minimum estimated time to damage ...," RP Memo RPG-140506-MEM-02, SLAC, May 2014.

[20] http://www.instron.us/en-us/our-company/library/glossary/s/stress-ratio, August 2017.

[21] Anonymous, *MILITARY HANDBOOK, METALLIC MATERIALS AND ELEMENTS FOR AEROSPACE VEHICLE STRUCTURES.* No. MIL-HDBK-5H, Dept of Defense, 1998.

[22] Z. Li. Slides, 2017.

[23] F. Kreith, *Principles of Heat Transfer*. Int. Textbook Co, 1967.

[24] M. Santana-Leitner, A. Ibrahimov, L. Nicolas, S. Rokni, D. Walz, and J. Welch, "Beam dumps of the new LCLS-II," Radiation Physics Note RP-14-13, SLAC, July 2014.

[25] J. Welch, "Beam Rastering System for the DUMPBSY," Physics Requirements Document LCLSII-2.7-PR-1028-R0, SLAC, June 2017.

[26] J. Blaha, "Activation analysis of the LCW systems for the LCLS-II high power CEBAF type dumps and associated shielding requirements," Radiation Physics Note RP-16-13, SLAC, November 2016.

[27] J. Blaha, "Shielding of LCLS-II main dumps for an operational envelope up to 8 GeV - evaluation of tritium production in soil, residual and prompt radiation," Radiation Physics Note RP-16-23-R2, SLAC, July 2017.

[28] D. Walz, D. Busick, T. Constant, K. Crook, D. Fryberger, G. Gilbert, J. Jasberg, L. Keller, J. Murray, E. Seppi, and R. Vetterlein, "Tests and description of beam containment devices and instrumentation - a new dimension in safety problems," SLAC Pub SLAC-PUB-1223, SLAC, March 1973.

[29] "Matweb, material property data," June 2017.

[30] D. Groeneveld, J. Shan, A. Vasic, L. Leung, A. Durmayaz, J. Yang, S. Cheng, and A. Tanase, "The 2006 CHF look-up table," *Nuclear Engineering and Design*, vol. 237, no. 15, pp. 1909 – 1922, 2007. NURETH-11.